Comparison of a Wide Magnet with a Conventional Magnet at 3 Tesla Magnetic Resonance Imaging Based on Signal Intensity Uniformity with Large Field of View: A Phantom Study

Ho-Beom Lee[1,3], Ji-Sung Jang[2,3], Yong-Soo Han[1,4], and Sung-Min Kim[1]*

[1]*Department of Medical Device Industry Dongguk University, 30, Pildong-ro 1-gil, Jung-gu, Seoul 04620, Republic of Korea*
[2]*Department of Bio-medical Science, Korea University, Sejong 30019145, Anam-ro, Seongbuk-gu, Seoul 30019, Republic of Korea*
[3]*Asan Medical Center, 88, Olympic-ro 43-gil, Songpa-gu, Seoul 05505, Republic of Korea*
[4]*Department of Radiological Science, Hanlym Polytechnic University, Chuncheon 24210, Republic of Korea*

Signal uniformity a criterion for providing objective information for evaluating the performance of a magnetic resonance imaging (MRI) and is an important measurement standard for evaluating the homogeneity of MRI system. In the early, magnet bore was very narrow in diameter. In general, magnetic bore was used with a small size that only allowed a brain imaging. Because, magnet bore size and homogeneity are inversely proportional. Recently, cylindrical-bore MR imagers with wider bores have been developed to provide higher field strengths. We compared the uniformity of large field of view (FOV) and image quality of large phantom imaging between spin echo (SE) and gradient echo (GRE) using 60-cm conventional-bore and 70-cm wide-bore 3.0 tesla (T) MR scanners. In the results, the SE and the GRE images demonstrated almost identical signal intensity patterns. The wide bore offers similar to uniformity in the large FOV compare with conventional bore. Wide-bore MRI using a large FOV can provide comparable image quality and geometric accuracy to conventional-bore MRI

Keywords : magnet bore, field homogeneity, magnetic resonance signal uniformity

1. Introduction

Static magnetic signal uniformity is a criterion for providing objective information for evaluating the performance of a magnetic resonance imaging (MRI) device and is an important measurement standard for evaluating the quality of MRI [1-5]. There are several factors that affect magnetic signal uniformity. The components of the MRI scanner include the main magnet bore system, radio frequency (RF) pulse transmitter, receiver and gradient coil. The magnet bore produces a uniformity static magnetic field along the z-direction. The magnetic signals emit maximum-strength electromagnetic waves immediately after excitation, but over time, the processing spins get out of synch, often due to differences in magnetic uniformity [6]. The important factors are magnetic strength, magnet bore size, gradient performance. In the early, magnet bore was very narrow in diameter and it only allowed a brain imaging as the homogeneity was inversely proportional to the bore size. More recently, cylindrical-bore MRI with wider and shorter bores have been developed to provide higher field strengths [7-9]. The first wide-magnetic bore systems appeared in the market around 2004. At that time, the poorer magnet uniformity and gradient performance were pointed out. Geometric accuracy unavoidably decreased in wide-bore MRI compared to that in conventional MRI. In particular, achieving sufficient geometric accuracy is problematic when using high-field wide-bore systems for abdominal, which covers a wide body area [10, 11].

Compared with a conventional-magnet bore 60-cm system, a wide-magnet bore system has reduced B_0 magnet homogeneity and uniformity. To solve this problem, MRI manufacturers use various RF subsystems to improve the magnet homogeneity. The results of clinical practice have showed that a 70-cm wide-magnet bore system has realized the perfect combination of the high-quality imaging with the patient comfort [12].

*Corresponding author: Tel: +82-2-3010-4325
Fax: +82-2-3010-6788, e-mail: sungmin2009@gmail.com

We compared the effect of magnet bore size (60-cm conventional-bore and 70-cm wide-bore) on the uniformity depending on the field of view (FOV) and geometric accuracy using spin echo (SE) and gradient echo (GRE) in 3.0-T MR scanners.

2. Materials and Methods

2.1. Phantom experiment study

Large phantom with a diameter of 40-cm included a section with a series of small circular holes arranged in a grid with separation of 50 cm. The phantom was filled with a copper sulphate solution, so that the holes showed up on MR images as hyper-intense point, which could be used to assess geometric accuracy over a large FOV.

2.2. Image acquisition

All MRI data were obtained using a 60-cm conventional-bore 3.0-Tesla (T) MR scanner with a 80 mT/m

maximum gradient strength and a 200 T/m/s maximum slew rate (Ingenia CX MRI, Philips Healthcare, Netherlands) that had a quadrature body coil and a 70-cm wide-bore 3.0-T MR scanner with a 45 mT/m maximum gradient strength and a 200 T/m/s maximum slew rate (Ingenia MRI, Philips Healthcare, Netherlands) that a quadrature body coil. Quadrature body coil (Philips Healthcare) were used for both acquisitions. Images were acquired using SE and GRE pulse sequences. In addition, we performed comparisons using different gradient amplitude performance.

In order to compare the uniformity of image intensity with different magnet bore size, SE weighted scanning parameters were as follow: FOV, 400 × 400; matrix size, 128 × 128; voxel size, 2 × 2; slice thickness 5-mm; flip angle, 90°; shortest repetition time (TR), shortest echo time (TE) and number of excitations, 1; gradients mode: regular, default, maximum.

GRE sequence parameters were as follow: FOV, 400 × 400; matrix size, 128 × 128; voxel size, 2 × 2; slice thick-

Table 1. Quantitative results of signal intensity in SE sequence.

Category		Regular	Default	Maximum
60 cm	50 %	1665.50 ± 29.10*	1676.34 ± 33.92*	1688.66 ± 38.28*
	75 %	1570.06 ± 52.31*	1578.93 ± 56.32*	1583.34 ± 64.86*
	100 %	1513.36 ± 76.77*	1522.76 ± 82.52*	1529.34 ± 79.92*
70 cm	50 %	1596.28 ± 30.10*	1602.34 ± 29.15*	1599.45 ± 34.58*
	75 %	1488.74 ± 55.71*	1501.42 ± 52.89*	1506.58 ± 56.39*
	100 %	1432.83 ± 75.36*	1445.65 ± 79.91*	1450.34 ± 83.92*

*vs signal intensity, p < 0.01
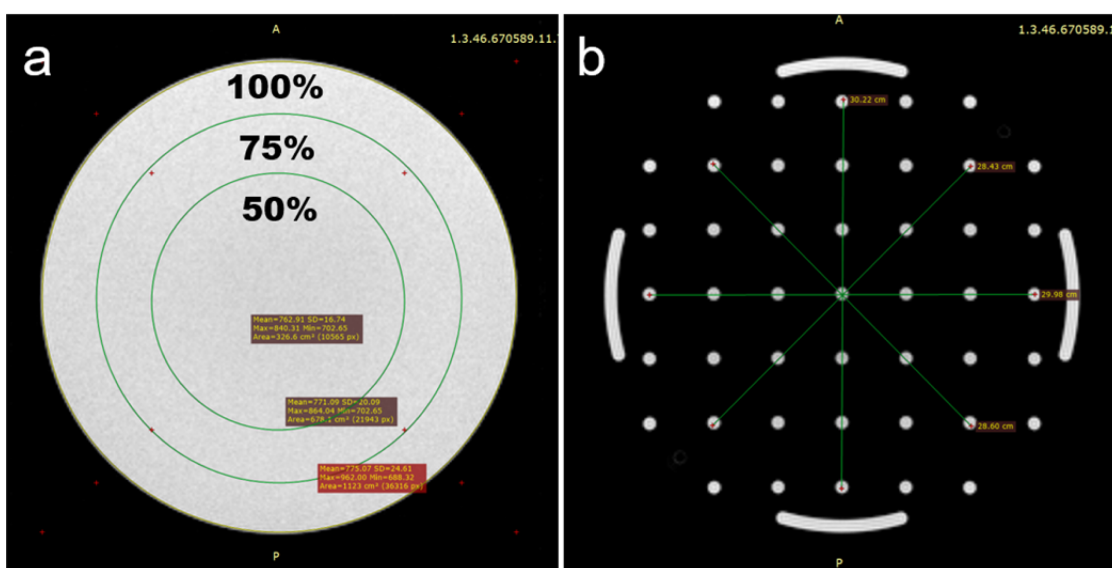$vs gradients mode, p < 0.01

Fig. 1. (Color online) (a) ROIs were placed over ACR phantom occupying 50 %, 75 % and 100 % of the area to measure the uniformity. (b) 4 lines were drawn for quality assurance method for geometric accuracy measurement.
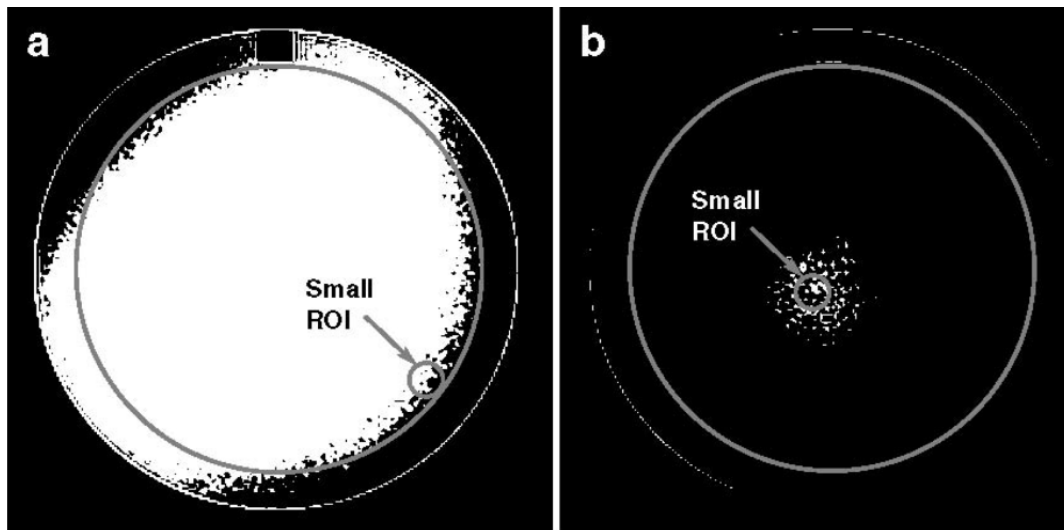
Fig. 2. Window setting and ROI placement for measurement of the low-signal value and high-signal value. ACR guidance given for PIU has been followed. (a) The ROI has been placed at what is visually estimated to be the largest 1 cm^2 dark area within the large ROI. (b) The ROI has been placed at what is visually estimated to be the largest 1 cm^2 bright area inside the large ROI. It can happen that rather than having a well-defined white region, one ends up with 1 or more diffuse areas of mixed black and white pixels. In that case, make a best estimate of the location of the brightest 1 cm^2 portion of the largest bright area.

ness, 5-mm; flip angle 10°; TR, TE: shortest, number of excitations, 1; gradient mode: regular, default, maximum. A detailed summary of the parameters is presented in Table 1.

2.3. Image analysis

We analyzed values called signal intensity, percent integral uniformity (PIU) and geometric accuracy which were both on the American College of Radiology (ACR) guidance to verify the MRI machine performance. For image analysis, the regions of interest (ROIs) were categorized into three ROIs corresponding 50 %, 75 %, and 100 % FOVs: 50 %, 75 %, and 100 % ROIs. The signal intensity values of 50 %, 75 %, and 100 % FOVs were calculated for each MR scanner using both SE and GRE pulse sequence with various gradients performance (Fig. 1). the phantom area were drawn followed by the window setting change to zero width and maximum window level that fills the FOV full of white signal. Increase the window level until the black signal appears inside the FOV. The first black signal intensity is measured as the lowest signal intensity. Decrease the window level until only small white signal lasts inside the FOV. The last remaining whites signal is measured as the highest signal intensity (Fig. 2). The highest and lowest signal values for each of the ACR series are combined to produce PIU using the following formula [10]:

$$PIU = 100 \times \left(1 - \frac{high - low}{high + low}\right)$$

MRI systems with 3.0-T systems should be greater than or equal to 82.0 %. Measurements were made according to the ACR phantom guide procedure on slice number 7.

The geometric accuracy was assessed by using a series of small circular holes where it could measure lengths over a large FOV. The diameter of the phantom was measured in four directions: top-to-bottom, left-to-right, and both diagonals.

2.4. Statistical Analysis

The statistical significance of the parametric data was determined using an analysis of variance (ANOVA). ANOVA value less than 0.01 was considered to indicate statistical significance. All statistical analysis was performed using the SPSS software package (version 18; SPSS, Chicago, IL, USA).

3. Results

Table 1, 2 compares the signal intensity values of images obtained on the conventional- and wide-bore scanners using various ROIs, sequences and gradients mode. The Signal intensity values of wide magnet bore were lower than the conventional magnet bore. There were statistically significant differences in signal intensity values for both sequences between the two bores (p < 0.05). However, signal intensity values on both bores showed a similar patterns and minor difference. With both scanners, the signal intensity values tended to decrease as ROI increased,

Table 2. Quantitative results of signal intensity in GRE sequence.

Category		Regular	Default	Maximum
60 cm	50 %	1521.52 ± 38.31*	1533.52 ± 35.49*	1550.34 ± 43.92*
	75 %	1257.22 ± 103.23*$	1386.39 ± 98.77*$	1425.04 ± 88.53*$
	100 %	973.36 ± 132.68*$	1113.76 ± 192.82*$	1288.29 ± 143.74*$
70 cm	50 %	1489.38 ± 43.10*	1506.61 ± 39.28*	1525.42 ± 37.38*
	75 %	1183.92 ± 65.77*$	1238.33 ± 66.32*$	1356.34 ± 43.92*$
	100 %	1023.54 ± 116.54*$	1158.46 ± 122.91*$	1256.34 ± 151.56*$

*vs magnet bore size and signal intensity, p < 0.01
$vs gradients mode, p < 0.01

with the signal intensity particularly high decreases at GRE sequence in both scanners. And the signal intensity values on both bores showed a maximum at the maximum gradient mode. There were no statistically significant differences in gradient mode for both sequences between the two bores (p > 0.05).

Table 3, 4 compares the PIU values of images obtained on the conventional- and wide-bore scanners using various ROIs, sequences and gradients mode. In constant, The PIU values of wide magnet bore were higher than the conventional magnet bore. There were statistically significant differences in the PIU values for both sequences between the two bores (p < 0.05).

Table 5 list the results of the geometrical accuracy measurements obtained on the conventional- and wide-bore scanners at various gradients mode and sequences.

There were no statistically significant differences in the measured lengths between the two bores (p > 0.05). In the geometry accuracy analysis, the wide magnet bore, There was no significant difference between the two sequences for either of the wide bore or conventional bore (p > 0.01), which meant the SE and the GRE images demonstrated identical geometry correction.

4. Discussion

In this study, we compared the signal intensity, uniformity and geometric accuracy of SE and GRE pulse sequences acquired on conventional-bore and wide-bore MRI scanners. We found that wide magnet bore (70-cm) had more PIU than conventional magnet bore (60-cm) on both sequences especially when FOV went larger. Regarding small area

Table 3. Quantitative results of PIU in conventional magnet bore.

	Category	50 % ROI	75 % ROI	100 % ROI
60 cm	SE			
	Regular	92.99 ± 0.63 %	92.23 ± 0.82 %	90.94 ± 0.75 %
	Default	93.66 ± 0.77 %	93.38 ± 0.85 %	90.03 ± 0.77 %$
	Maximum	93.75 ± 0.58 %$	92.76 ± 0.75 %$	90.55 ± 0.87 %$
	GRE			
	Regular	91.96 ± 0.98 %	86.10 ± 0.93 %	82.22 ± 0.96 %
	Default	92.53 ± 0.93 %$	88.47 ± 0.72 %$	85.41 ± 0.85 %$
	Maximum	92.69 ± 1.13 %$	89.39 ± 0.90 %$	87.83 ± 0.65 %$

*vs magnet bore size and PIU, p < 0.01
$vs gradients mode, p < 0.01

Table 4. Quantitative results of PIU in wide magnet bore.

	Category	50 % ROI	75 % ROI	100 % ROI
70 cm	SE			
	Regular	92.65 ± 0.58 %	91.75 ± 0.75 %	90.88 ± 0.83 %
	Default	92.19 ± 0.95 %	91.48 ± 0.66 %	91.04 ± 1.05 %
	Maximum	92.85 ± 1.12 %	92.03 ± 0.83 %	91.11 ± 1.13 %
	GRE			
	Regular	91.25 ± 1.52 %	87.23 ± 1.23 %	85.35 ± 1.15 %
	Default	91.96 ± 1.35 %	88.47 ± 1.45 %	87.41 ± 0.83 %
	Maximum	91.87 ± 0.98 %	90.58 ± 0.88 %	88.23 ± 1.05 %

*vs magnet bore size and PIU, p < 0.01
$vs gradients mode, p < 0.01

Table 5. Quantitative results of geometric accuracy in two groups.

Category			Regular	Default	Maximum
60-cm	SE	Top-to-bottom	30.22 ± 0.13	30.31 ± 0.18	30.26 ± 0.15
		Left-to-right	30.03 ± 0.11	29.89 ± 0.15	30.17 ± 0.14
		Right-diagonal	28.83 ± 0.09	28.88 ± 0.11	28.92 ± 0.15
		Left-diagonal	29.02 ± 0.16	28.93 ± 0.14	28.58 ± 0.21
	GRE	Top-to-bottom	29.89 ± 0.21	30.15 ± 0.15	30.35 ± 0.17
		Left-to-right	29.91 ± 0.19	30.53 ± 0.18	30.98 ± 0.16
		Right-diagonal	29.15 ± 0.11	28.94 ± 0.13	29.03 ± 0.22
		Left-diagonal	28.92 ± 0.18	28.96 ± 0.14	29.31 ± 0.18
70-cm	SE	Top-to-bottom	30.16 ± 0.14	30.28 ± 0.20	30.19 ± 0.17
		Left-to-right	29.88 ± 0.18	29.97 ± 0.17	30.08 ± 0.19
		Right-diagonal	28.66 ± 0.13	28.98 ± 0.17	28.96 ± 0.19
		Left-diagonal	28.99 ± 0.19	29.02 ± 0.16	2.31 ± 0.18
	GRE	Top-to-bottom	30.58 ± 0.16	29.95 ± 0.14	30.43 ± 0.15
		Left-to-right	30.18 ± 0.15	30.23 ± 0.17	29.91 ± 0.16
		Right-diagonal	29.06 ± 0.13	29.02 ± 0.18	28.96 ± 0.12
		Left-diagonal	28.88 ± 0.15	28.97 ± 0.17	28.98 ± 0.16

*vs magnet bore size and geometry accuracy, $p < 0.01$
$vs gradients mode and geometry accuracy, $p < 0.01$

(50 %-FOV) and large area (100 %-FOV), PIU is the degree of lack of static magnetic field homogeneity, uniformity for example the fractional deviation of the local magnetic field from the average value of the field. The expected precession frequency only exists in the center of the imaging volume. The homogeneity failure could be observed in the frequency specific fat saturation pulses become less effective when the FOV is increased. The same problem appears when objects distant from the isotropic center in left-right direction or FOV is too large. The variation of PIU of our study was significantly higher in the wide-magnet bore compared to that of conventional-magnet bore which proved the unavoidable in magnetic field homogeneity produced by the scanner as well as by object susceptibility decreased as the FOV became large as more tissues were imaged and the precession frequencies changed more across the imaging volume [3, 15]. There were no differences between the two profiles and they showed a high reproducibility. Also, the SE and the GRE images showed almost identical geometric accuracy pattern which had no significant difference on either of the wide bore or conventional bore ($p > 0.01$). These two sequences is routinely used in all anatomical regions for modern MR imaging, And all other sequence used in MR are variations of these from adding on different parameters.

In previous study, the geometric accuracy is unavoidably worse with wide-bore MR than with conventional MRI. Some researchers have reported that geometric accuracy

difference caused by gradient nonlinearity is small in the center of the magnet, and achieving high geometric accuracy becomes problematic when imaging a large FOV area using high-field wide-bore MRI systems [18, 19]. This can be explained by radiofrequency field (B_1) inhomogeneity and RF shimming. B1 inhomogeneity arises because the RF power is absorbed differently across the patient, due to the changing permittivity and conductivity of tissues (dielectric effects), and standing waves in tissues. This causes a variable flip angle across the patient, which can lead to dielectric shading, seen more at 3T. To improve this, RF shimming is the process of using multiple RF transmission sources to compensate for variable flip angle across the field-of-view.

Our experiments demonstrated that the PIU values equal to both bores as the FOV increased in both sequences. Although the signal intensity value between the two bores were minor difference, regardless of the large FOV, PIU remained similar with the wide magnet-bore was greater than that with the conventional bore. Given our findings, wide-bore MRI using a large FOV can be considered a useful technique. For example, some patients who need an MRI exam are anxious about the process, fearing they will be claustrophobic in the magnet bore. Wide magnet-bore can create an atmosphere that examination them out of the imaging suite and into a relaxing environment of their choice.

Our study has some limitations. The gradients performance influences the minimum attainable TR and TE for

magnetic signal intensity. Especially, GRE influences the echo spacing between wide magnet and conventional magnet. Because of the both scanners parameters are not identical as GRE sequence. However, the only difference is the TR and TE values according to gradients performance. And we didn't use a various receiver body coil. We only used quadrature-coil. Therefore, a further study needs to be measured with a various receiver coil. Nevertheless, we demonstrate the wide bore offers similar to uniformity in the large FOV compare with conventional bore.

5. Conclusion

To conclude, the wide bore offers similar to uniformity in the large FOV compare with conventional bore. Wide-bore MRI using a large FOV can provide comparable image quality and geometric accuracy to conventional-bore MRI.

References

[1] E. K. Insko, T. J Connick, M. D. Schnall, and S. G. Orel, Magn. Reson. Med. **37**, 5 (1997).

[2] O. Dietrich, J. G. Raya, S. B. Reeder, M. F. Reiser, and S. O. Schoenberg, Journal of Magnetic Resonance Imaging: An Official Journal of the International Society for Magn. Reson. Med. **26**, 2 (2007).

[3] H. Nakazawa, M. Komori, Y. Shibamoto, Y. Takikawa,, Y. Mori, and T. Tsugawa, Med. Imaging Radiat. Oncol. **58**, 5 (2014).

[4] X. Chen and J. Dai, Appl. Clin. Med. Phys. **19**, 3 (2018).

[5] S. Saito, K. Tanaka, and T. Hashido, Radiol. Phys. Technol. **9**, 2 (2016).

[6] J. Wang, M. Qiu, Q. Yang, M. Smith, and R. Todd Con-

stable, Magn. Reson. Med. **53**, 2 (2005).

[7] E. F. Jackson, American Association of Physicists in Medicine Annual Meeting (2009).

[8] P. Keller, Metrolab Instruments. Geneva: Metrolab Instruments (2007).

[9] G. C. Wiggins, J. R. Polimeni, A. Potthast, M. Schmitt, V. Alagappan, and L. L. Wald, Magn. Reson. Med. **62**, 3 (2009).

[10] American College of Radiology, Magnetic Resonance Imaging Quality Control Manual (American College of Radiology, Restoe, VA, 2004).

[11] S. Hadjidemetriou, C. Studholme, S. Mueller, M. Weiner, and N. Schuff, Medical Image Analysis **13**, 1 (2009).

[12] B. R. Condon, J. Patterson, D. Wyper, A. Jenkins, and D. M. Hadley, Br. J. Radiol. **60**, 709 (1987).

[13] A. Ogura, H. Inoue, M. Higashida, M. Yamazaki, and T. Uto, Nippon Hoshasen Gijutsu Gakkai Zasshi **53**, 12 (1997).

[14] B. Belaroussi, J. Milles, S. Carme, Zhu, Y. M., and H. Benoit-Cattin, Medical Image Analysis **10**, 2 (2006).

[15] H. Nakazawa, M. Komori, Y. Shibamoto, Y. Takikawa, Y. Mori, and T. Tsugawa, Med. Imaging Radiat. Oncol. **58**, 5 (2014).

[16] J. Stattaus, S. Maderwald, M. Forsting, J. Barkhausen, and M. E. Ladd, Magn. Reson. Med. **27**, 5 (2008).

[17] A. Arepally, P. V. Karmarkar, D. Qian, B. Barnett, and E. Atalar, J. Vasc. Interv. Radiol. **17**, 7 (2006).

[18] D. Wang, W. Strugnell, G. Cowin, D. M. Doddrell, and R. Slaughter, Magn. Reson. Imaging. **22**, 211 (2004).

[19] C. P. Karger, A. Hoss, R. Bendl, V. Canda, and L. Schad, Phys. Med. Biol. **51**, 253 (2006).

[20] L. M. Harris, J. Robinson, and R. G. Menzies, Behav. Res. Ther. **37**, 2 (1999).

[21] C. Bangard, J. Paszek, F. Berg, G. Eyl, J. Kessler, K. Lackner, and A. Gossmann, Eur. J. Radiol. **64**, 1 (2007).